ARTICLES
https://doi.org/10.1038/s41593-019-0406-3
nature neuroscience

High-order coordination of cortical spiking activity modulates perceptual accuracy

Neda Shahidi[1,2], Ariana R. Andrei[1], Ming Hu[1,3] and Valentin Dragoi[1*]

The accurate relay of electrical signals within cortical networks is key to perception and cognitive function. Theoretically, it has long been proposed that temporal coordination of neuronal spiking activity controls signal transmission and behavior. However, whether and how temporally precise neuronal coordination in population activity influences perception are unknown. Here, we recorded populations of neurons in early and mid-level visual cortex (areas V1 and V4) simultaneously to discover that the precise temporal coordination between the spiking activity of three or more cells carries information about visual perception in the absence of firing rate modulation. The accuracy of perceptual responses correlated with high-order spiking coordination within V4, but not V1, and with feedforward coordination between V1 and V4. These results indicate that while visual stimuli are encoded in the discharge rates of neurons, perceptual accuracy is related to temporally precise spiking coordination within and between cortical networks.

Perception relies on successive transformations of sensory inputs within local and long-range cortical networks. While the classical view of sensory coding in the neocortex revolves around the idea that information is encoded in neuronal firing rates[1,2], whether the relative timing of spike discharges is functionally significant remains poorly understood. Previous theories have proposed that the precise temporal coordination of neuronal activity within cell populations, including multilayer synchronous spikes as an effective signaling mechanism[3–6], information encoding via coordinated spiking[5,7,8], synchronous oscillations[9], and efficient driving of postsynaptic targets[10], influences the efficacy of neuronal communication and perceptual accuracy. In reality, the idea that precise temporal coordination of neuronal spiking influences cortico-cortical communication and behavioral performance has received little empirical support[11].

One possible function of spiking coordination, persistently proposed in neuroscience studies over the past two decades, is to increase the firing rates of target neurons via the temporal integration of spikes[10]. Indeed, several studies have shown that cortical neurons fire vigorously when thalamic cells emit synchronous spikes[12,13]. However, this idea has been challenged by theoretical work[14] proposing that while cortico-cortical signaling relies on excitatory cells, the activity of these neurons is often correlated with inhibitory responses[15–17]. Thus, spiking coordination could cause an increase in local inhibition that would reduce the enhancing effect of temporal summation of excitatory responses[18]. Furthermore, most studies linking temporal coordination to the firing of postsynaptic targets were performed in anesthetized animals. Importantly, anesthesia has been associated with synchronized brain states that might influence coordinated spiking[19]. In awake animals, there is far less evidence to indicate that temporal coordination of spiking activity is functionally relevant for behavior. Whereas cortico-cortical synchrony of local field potentials (LFPs) and spike–LFP interactions[20–22] have been related to aspects of coding and behavior, LFPs represent an indirect measure of spiking activity[23]. Therefore, the functional significance of spiking coordination during wakefulness remains poorly understood.

We reasoned that a limitation of previous studies performed in awake animals is the fact that coordination has been examined exclusively on the basis of pairwise correlations while ignoring higher-order coordination among triplets, quadruplets, and larger groups of cells. This raises the possibility that examining higher-order coordination in the timing of spike discharges among neurons within cell assemblies could uncover an influence on sensory coding and perception. Here, we examined whether and how the coordination of spiking activity in the early and mid-level visual cortex (areas V1 and V4) of behaving monkeys is related to neural coding and perceptual accuracy. We discovered that spiking coordination among groups of three or more cells is time locked to stimulus presentation and carries information about perceptual reports. Specifically, perceptual accuracy correlated with higher-order spiking coordination in V4, but not V1, and with feedforward coordination between the early and mid-level visual cortex. These results provide mechanistic insight into the role of spiking coordination within visual cortical populations and its relationship to perception.

Results

We recorded ensemble spiking activity in the early and mid-level visual cortex (areas V1 and V4 of macaque monkeys) using 16-channel linear array microelectrodes that were arranged so as to ensure a substantial overlap (approximately 80%) between the receptive fields of the cells recorded in the two areas[24,25] (Fig. 1c; Methods). To examine whether high-order neuronal coordination events occur during cognitive behavior, we trained monkeys to signal whether two successively flashed natural scenes were identical or different ($n = 26$ sessions, see Methods). In each trial, two identical images (target and test, 8–10° in diameter) were flashed for 300-ms each, and were separated by a variable 500–1,200-ms delay. The test image was rotated by 0° (match condition) or by 3–5° (non-match condition) with respect to target (Fig. 1a). The non-match orientation difference was near the discrimination threshold of the animal (Fig. 1b), measured in separate behavioral experiments before the start of electrophysiological recordings. The behavioral

[1]Department of Neurobiology and Anatomy, McGovern Medical School, University of Texas, Houston, TX, USA. [2]Present address: Department of Ophthalmology, Universitätsmedizin Göttingen, Göttingen, Germany. [3]Present address: Department of Brain and Cognitive Sciences, Massachusetts Institute of Technology, Cambridge, MA, USA. These authors contributed equally: Ariana R. Andrei, Ming Hu. *e-mail: v.dragoi@uth.tmc.edu

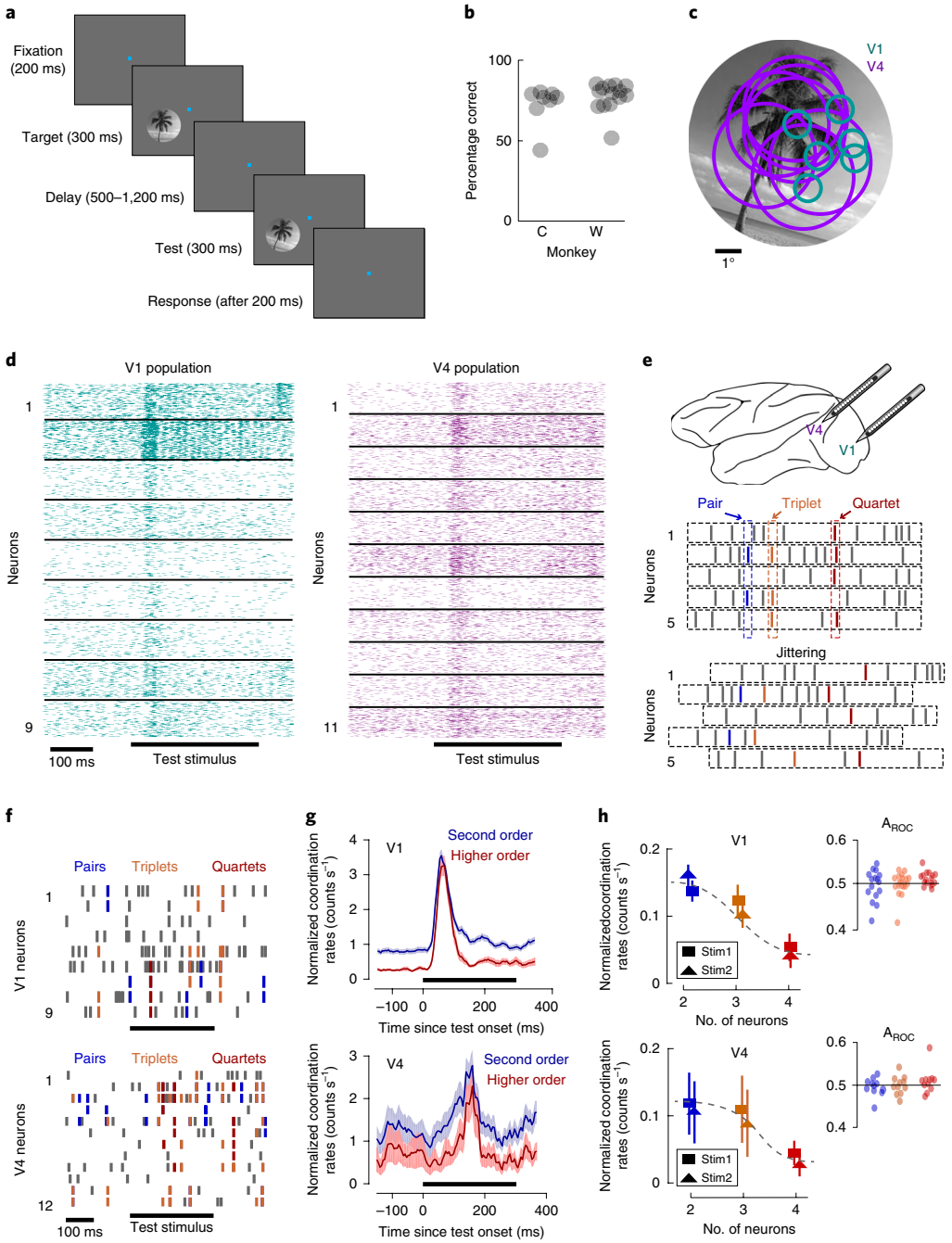

Fig. 1 | High-order coordination in spiking activity during a behavioral task. a, Delayed match-to-sample image discrimination task. Animals were trained to report whether two briefly flashed successive natural scenes (target and test) were identical or different. **b**, Behavioral performance of two animals (monkey W: 12 sessions; monkey C: 14 sessions), with monkey W achieving 60 ± 5% (mean ± s.e.) correct responses in non-match trials, while monkey C achieved 73 ± 7% correct responses in non-match trials. The chance level is 50% for combined match and non-match trials. **c**, Receptive field positions of individual V1 and V4 neurons recorded simultaneously in a representative session are shown with reference to the image stimulus. **d**, Raster plots of spiking activity of simultaneously recorded neurons in V1 and V4. The horizontal black bars represent the time of test stimulus presentation. **e**, Top: cartoon showing coordinated spike events in groups of two or more neurons. Middle and bottom: sample pair, triplet, and quartet coordination. Coordination rates in jittered spike trains were used as the null hypothesis to determine the statistical significance of coordinated spiking. **f**, Raster plots of 9 V1 and 12 V4 cells in 1 trial overlapped with coordinated spiking for pairs, triplets, and quartets. The horizontal black bars mark the presentation of the test stimulus. **g**, PSTH of second order (pairs) and higher-order (triplets and above) coordinated events for the entire dataset within a 300-ms stimulus window shifted in 20-ms increments (average of 22 V1 and 12 V4 sessions). The rates were normalized within each session to avoid bias toward sessions with a larger number of neurons. Shaded areas represent the s.e.m. **h**, Jitter-corrected normalized coordination rates in V1 and V4 during the presentation of each test stimulus (stim1 and stim2) as a function of ensemble size. The analysis window was 0–300 ms after the test onset. Error bars represent the s.e.m. across sessions (V1: 22 sessions; V4: 14 sessions). Inset: A_{ROC} for stim1 and stim2 trials averaged across coordinated events of order 2, 3, and 4 shown for each session. Each data point represents one session.

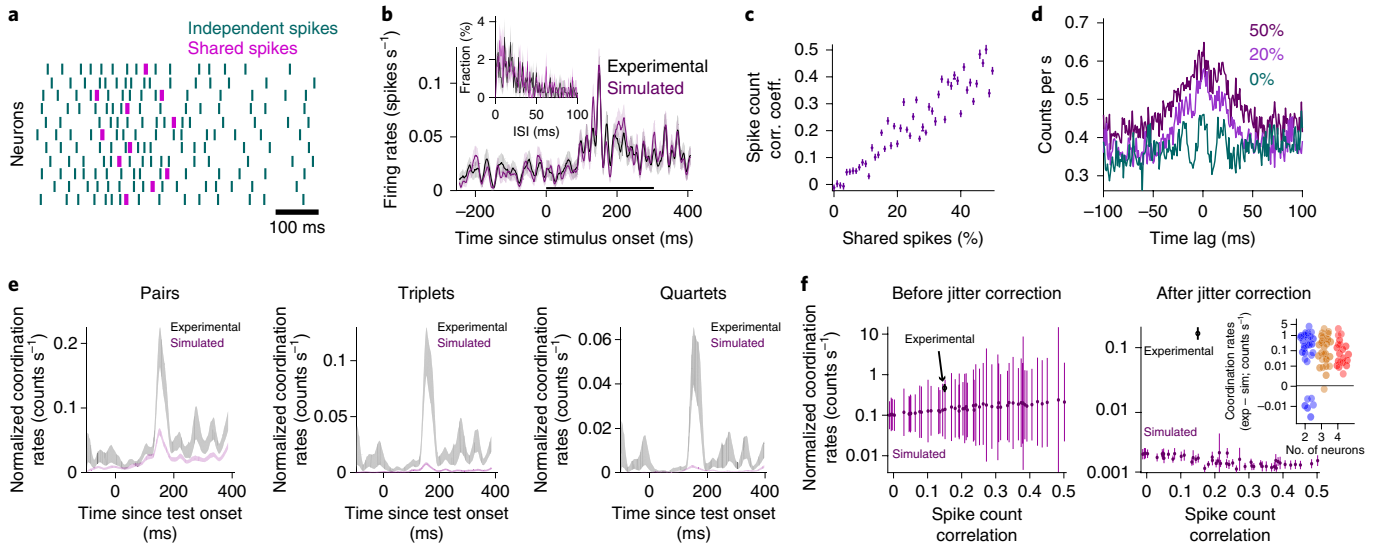

Fig. 2 | Simulation of correlated spike trains with statistics similar to those from recorded neurons, except for coordinated spiking. a, Spike trains of simulated neurons generated using independent Poisson processes, and shared spikes that increase the spike count correlation without increasing spike-time correlations (shared spikes are within the same 25-ms window, whereas coordinated spikes are within the same 5-ms window). **b**, Trial-averaged histogram of spike counts ($n = 200$) shown for an interval from 200 ms before stimulus onset to 500 ms after stimulus onset for a real and simulated neuron. The black bar represents the interval of test stimulus presentation. Inset: histogram of the inter-spike time interval (ISI) for one experimental neuron and its corresponding simulated neuron. For all the neurons in our population, the distributions of inter-spike time intervals for the simulated neurons matched the experimental ones (two-sided Kolmogorov–Smirnov test, $P > 0.68$). Shaded areas represent the s.e.m. across trials. **c**, Correlation coefficients (corr. coeff.) of spike counts across trials ($n = 200$) averaged for all the pairs ($n = 66$) of the simulated population as a function of the percentage of shared spikes. **d**, CCG averaged across trials and pairs for the neural population for different percentages of shared spikes. **e**, PSTH of coordinated rates for experimental and simulated neural populations shown separately for pairs, triplets and quartets. The spike count correlation within the simulated population was matched to that of the real population using the regression fit from **c**. Shaded areas represent the s.e.m. across trials ($n = 200$). **f**, Left: raw coordinated rates averaged for all neuronal assemblies (combining size 2 to 12), regardless of the significance of their occurrence, for the simulated and experimental spike trains. Right: coordination rates from the left panel after subtracting the coordination rates of surrogate data generated by jittering the spike trains (jitter range = 10 ms) for the simulated and experimental spike trains. The simulation was repeated 100 times for each data point. Data points represent the trial average ($n = 200$); error bars represent the s.e.m. Inset: the difference between coordination rates of experimental (exp) and simulated (sim) populations for our 34 recording sessions.

performance of the two animals was as follows for non-match trials: monkey W: 60 ± 5% correct responses; monkey C: 73 ± 7% correct responses. For match trials, the results were as follows: monkey W: 85 ± 5% correct responses; monkey C: 87 ± 3% correct responses. Both stimuli fully covered the receptive fields of the neurons recorded simultaneously in each session (Fig. 1c).

Detection of coordinated spiking events. We analyzed the spiking activity of 293 single neurons (up to 14 cells per area in each session) that were significantly modulated by the stimuli in our experiments (Fig. 1d). We detected coordinated spiking by computing the frequency of co-occurrence of spike events[3,26] for neural populations of different sizes in each area (see Methods). Briefly, we calculated the frequency of near-coincident (5-ms) firing of two or more neurons that occurred significantly more often than expected by chance on a trial-by-trial basis (for an example, see Fig. 1e). We also defined the order of a coordinated event as the number of neurons simultaneously spiking within the time bin of the event. Note that this definition does not provide insight into the nature of the interaction between the neurons within an ensemble[27].

Coordination rates were calculated by dividing the number of coordinated event occurrences by the time length of the analysis window and the total number of possible neuron combinations (see Methods). Statistical significance was tested against the null hypothesis generated by jittering spike trains (Fig. 1e; the jitter range was ±10 ms for 20 jittering iterations)[26]. Jittering preserves all statistics with a coarser time scale than the jittering window, including periodic oscillations, co-fluctuations of firing rates, and trial-by-trial variability, but not the precise timing of spikes. Therefore, subtracting coordination rates of jittered spike trains from those of the original data (before assessing statistical significance) rules out the contribution of coherent oscillations or co-fluctuations of firing rates[26].

Coordinated events are time locked to visual stimuli. To characterize neuronal coordination, we analyzed a total of 4,826 statistically significant neuron combinations that generated coordinated spiking ($P < 0.01$, Wilcoxon signed-rank test with false discovery rate (FDR) multiple comparison correction[28]), including 310 pairs, 1,332 triplets, and 3,184 quartets. The average percentage of neuronal combinations that generated significant events was 46% for pairs, 40% for triplets, and 42% for quartets. Examples of V1 and V4 population spike trains (Fig. 1f) revealed that coordination between two, three, and four spikes is not a random event, but is frequently encountered during stimulus-evoked responses. Importantly, comparing the auto-correlograms and cross-correlograms (CCGs) of spike trains in epochs containing significantly coordinated spiking with those in the pre-stimulus interval (Supplementary Fig. 1) did not reveal signs of periodic oscillations of population activity. This indicates that precise spike coordination is unrelated to coherent oscillations[9]. The total number of significantly occurring coordinated events ($P < 0.01$) did not differ between the two cortical areas (Supplementary Fig. 2). Across sessions, a pronounced increase in coordination rates was time locked to the stimulus onset (Fig. 1g); however, coordination rates in V1 or V4 were unrelated to the

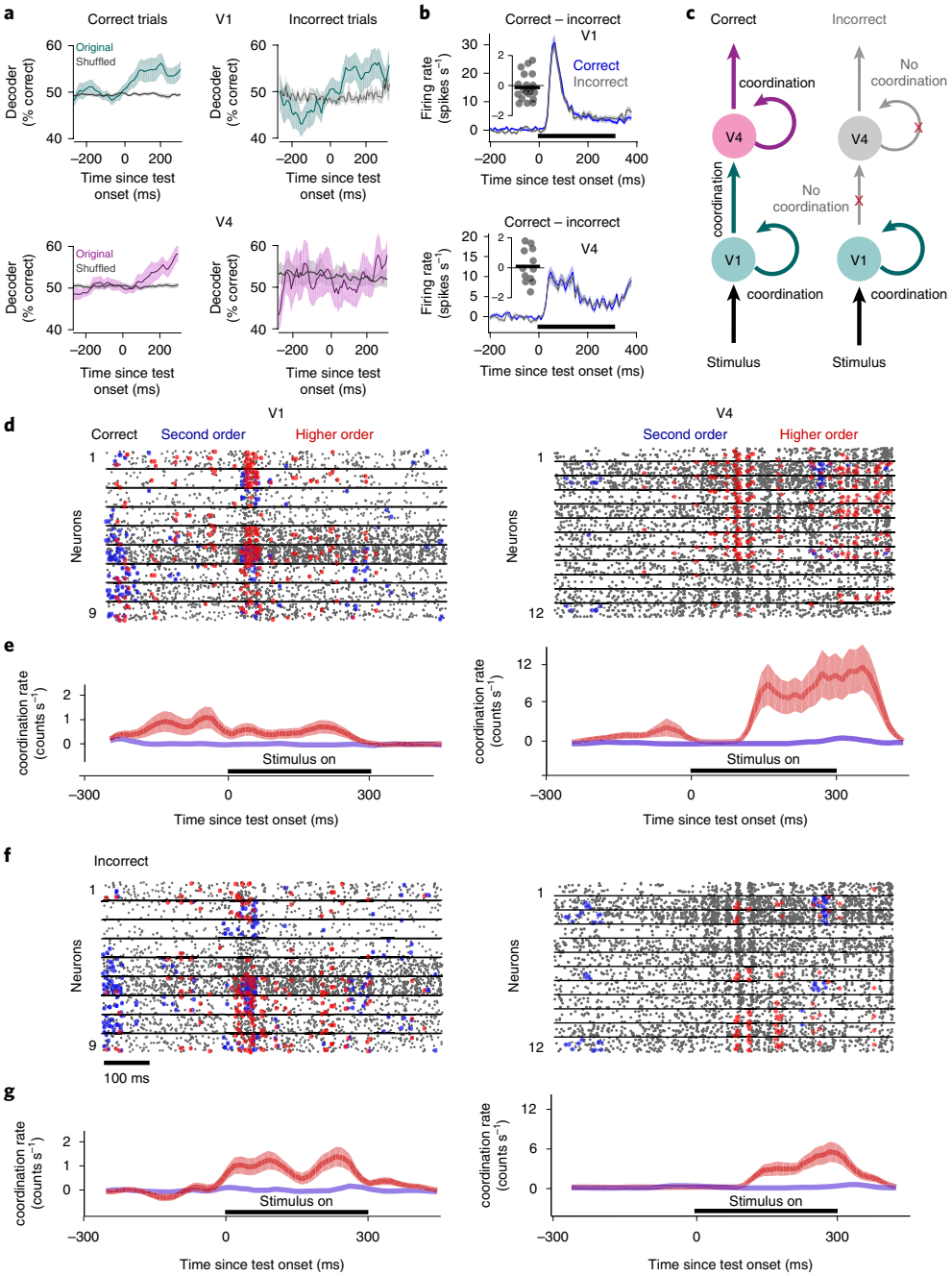

Fig. 3 | Relationship between high-order coordination rate and perceptual accuracy. a, Performance of a classifier that uses firing rates of all simultaneously recorded neurons in V1 and V4 to decode the test stimulus (we used a 200-ms window sliding in 20-ms increments). The classifier was trained using 80% of all correct trials, and performance was validated by classifying the remaining 20% of trials (performance was cross-validated 1,000 times by randomly dividing trials to training and test sets). Shuffled classifier trial labels (stim1 versus stim2) were shuffled before training, and then the cross-validation procedure was repeated. Shaded areas represent the s.e.m. across 22 sessions in V1 and 12 sessions in V4. **b**, Baseline-removed population-averaged PSTHs of all the neurons in V1 ($n=183$) and V4 ($n=110$) averaged for correct and incorrect non-match trials separately during the test stimulus presentation. The bin size was 20 ms. Shaded areas represent the s.e.m. Insets: the difference of the mean population firing rate (correct versus incorrect trials) in V1 and V4. Circles represent individual sessions. **c**, Cartoon describing our conceptual model, whereby V4 neurons decode the information from upstream areas (including V1). Spiking temporal coordination controls perceptual accuracy by modulating the efficacy of cortico-cortical signaling. **d**,**f**, Raster plots of 9 V1 and 12 V4 cells from a single session for correct (**d**) and incorrect (**f**) trials. Overlaid are second-order or higher-order spiking coordinated events generated by significant neuron combinations, subsampled for clarity with an equal number of randomly selected trials showing patterns for which the frequency of occurrence was significantly different between correct and incorrect sets ($P<0.01$, two-sided Wilcoxon rank-sum test). The horizontal black lines mark the presentation of the test stimulus. **e**,**g**, Jitter-corrected coordination rates in V1 and V4 (before normalization) representing the frequency of occurrence of coordinated events for correct (**e**) and incorrect (**g**) trials in each area calculated for a 300-ms window sliding every 10 ms. Negative numbers represent an original coordination rate < shuffled rate. The traces represent the average across trials ($n=46$) and shaded areas represent the s.e.m.

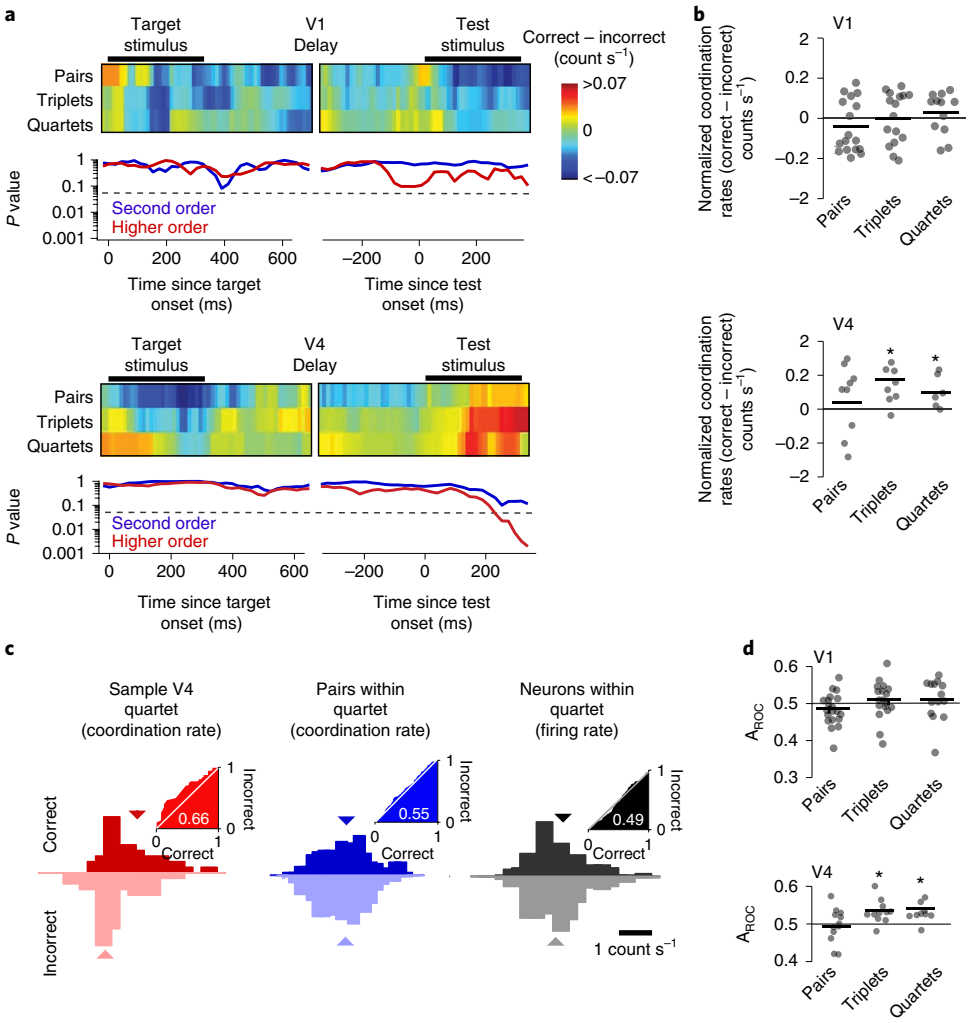

Fig. 4 | Population effects: correct trials are associated with higher order coordination in area V4. a, Top panels: the difference in coordination rates (for pairs, triplets, and quartets) between correct and incorrect trials measured using a 300-ms window shifted in 10-ms increments (average of sessions; $n=22$ for V1 and $n=12$ for V4). The small gap during the delay period is due to the variable interval between target and test. Bottom panels: statistical significance of the two-sided Wilcoxon signed-rank test (*P* value) for the difference in coordination rates between correct and incorrect trials. Triplets and quartets are combined as 'higher-order' coordination events. The broken lines mark the significance threshold of the *P* value (0.05). **b**, Normalized coordination rates for pairs, triplets, and quartets, measured for the 300-ms window starting 150 ms after test onset (circles represent individual sessions). A hyperbolic scale was used for the *y* axis to optimize representations for all sessions ($n=22$ for V1 and $n=12$ for V4). The bar shows the average across sessions. The asterisks indicate statistical significance (see Methods). **c**, The distribution of coordination rates for (left) correct and incorrect trials for a sample quartet, (middle) all six possible pairs within the quartet, and (right) the firing rates of all four neurons within the quartet. Insets: ROC curves for correct versus incorrect trials. **d**, A_{ROC} for correct versus incorrect trials averaged across all coordination events of the same order (pairs, triplets, quartets) within each session (circles represent individual sessions).

stimulus orientation for any size of the neural assemble (Fig. 1h, $P>0.1$; coordination rates were calculated during the 300-ms test stimulus presentation).

We further examined the relationship between coordinated events and test stimulus orientation using receiver operating characteristic (ROC) analysis. Can stimuli be decoded from the coordination rates associated with neuron pairs, triplets, and quartets? The area under the ROC curve (A_{ROC}) is typically used to determine the performance of a binary classifier discriminating between two conditions[29]. As shown in the insets in Fig. 1h, the A_{ROC} for ensembles of various sizes is not significantly different from 0.5 ($P>0.1$) in either V1 or V4, which indicates that stimulus encoding is unrelated to precise temporal coordination of neuronal spiking. We then used support vector machine decoders to decode stimulus identity from the coordination rates of neuronal pairs, triplets, and quartets calculated during test stimulus presentation. However, this analysis indicated that coordination rates cannot be used to decode stimulus information better than chance in any of the two areas ($P=0.8$; Supplementary Fig. 3). These results are consistent with the long-standing idea that stimulus-specific information in the neocortex is transmitted by firing rate modulations and not by spike timing coordination[2].

The fact that stimulus presentation increases firing rates in the presence of long timescale correlations raises the issue of whether the observed coordination rates exceed those expected given the statistics of population activity. We therefore generated simulated spike trains with the same response statistics as our recorded neurons, and subsequently computed coordination rates while varying the co-fluctuation of spike counts (Fig. 2a; Methods) such that spike count and spike time correlations increased monotonically with the percentage of shared spikes (Fig. 2c,d). As shown in Fig. 2b, the trial-averaged firing rates and inter-spike time distributions

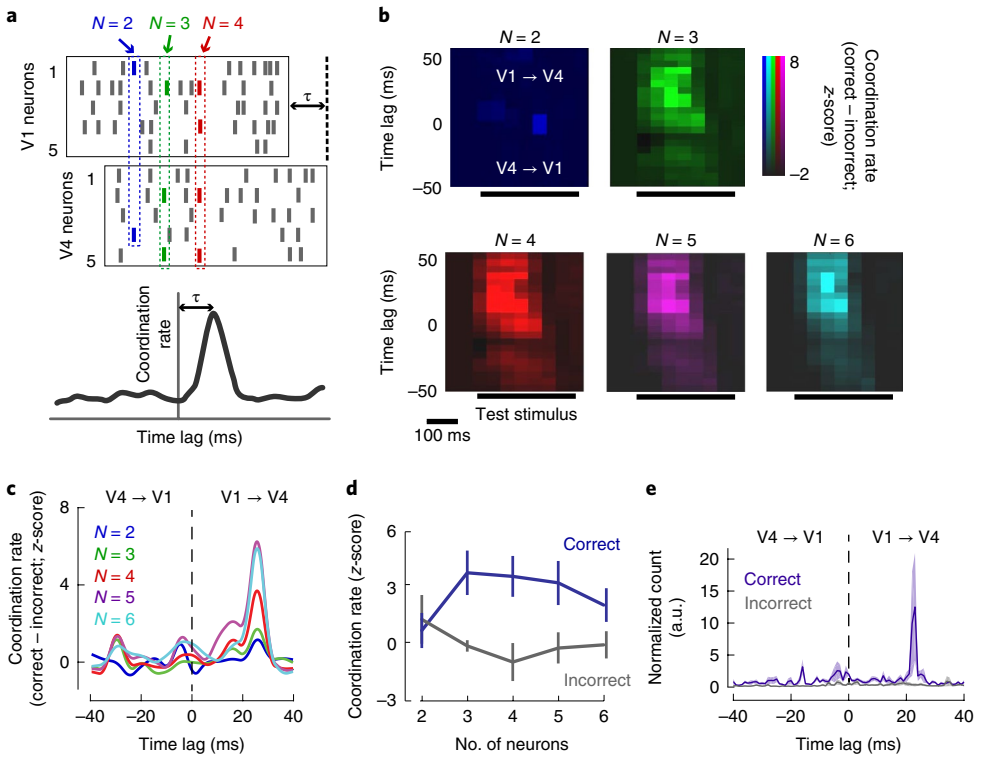

Fig. 5 | Feedforward coordination between V1 and V4 neurons is related to perceptual accuracy. a, Cartoon raster plots of V1 and V4 responses illustrating the magnitude and time lag of V1–V4 coordination. Coordination rates were calculated from spike trains from both areas by shifting the V4 spikes by time lag τ (between ±40 ms, in 5-ms steps). The peak coordination and time lag were determined after *z*-scoring coordination rates for all time lags by the average coordination rate of the tail (−40 to −20 time lag). **b**, Difference between coordination rates for correct and incorrect trials averaged across 8 sessions as a function of time lag. The peak coordination rate (*z*-score > 2) for higher-order coordinated events occurs when V4 lags V1 by +25 ms and around 100 ms after test onset. **c**, Coordination rate (correct versus incorrect) as a function of time lag for each event size was calculated for the 300-ms window overlapping the test stimulus presentation. The peaks for higher-order coordinated events occur for feedforward communication (20- to 40-ms time lags; the average time lag across sessions was 25 ms). **d**, The *z*-scored coordination rates for correct and incorrect trials, calculated for the time lag corresponding to the peak in each session (we included 7 of 8 sessions showing a significant difference between correct and incorrect trials; data points represent averages across sessions; $P = 0.016$, two-sided Wilcoxon signed-rank test). **e**, CCG of the occurrence times of higher-order events in V1 and V4 for correct and incorrect trials (5-ms bin size). The rates of co-occurrence of higher-order events in V1 and V4 were normalized by the geometric mean of the occurrence rates. Error bars represent the s.e.m. across sessions ($n = 8$).

of simulated neurons matched those of the corresponding recorded neurons ($P = 0.6$, Wilcoxon signed-rank test, and $P = 0.68$, Kolmogorov–Smirnov test, respectively). We further confirmed that coordination rates associated with the simulated neural population are lower than the degree of coordination expected by chance. That is, the coordination rates of simulated spike trains, calculated by combining pairs, triplets, and quartets, were more than five times lower than coordination rates of real neurons (Fig. 2e). For 100 repetitions of simulated populations, each with 0–50% shared spikes, we identified less than 0.002 coordinated events per second; that is, about 50 times lower than the coordination rates in the actual neuronal population (Fig. 2f). Across sessions, we found higher coordination rates in experimental data compared to simulated populations for high-order events in 33 out of 34 sessions in V1 and V4 ($P = 1.8 \times 10^{-6}$, Fig. 2f, inset). For pairs of neurons, 28 out of 34 sessions exhibited significantly higher coordination rates compared to simulated spike trains ($P = 8.5 \times 10^{-4}$). This is expected given the higher chance of false-positive coordination for pairs of cells[26].

Decoding the population firing rates. Since stimulus orientation is unrelated to spiking coordination, we further examined whether the firing rates of the neural populations in V1 and V4 can be used to decode the stimuli in the task. That is, discriminate between the two images (rotated or not) separately for 'correct' and 'incorrect' trials. There were two issues of interest: (1) could the two stimuli, identical in structure but slightly rotated with respect to each other, be decoded from the population firing rates? (2) Is stimulus information in each area related to the behavioral performance of the animal? We decoded the population response in each session by using the firing rates of neurons elicited by the test stimuli (174 cells in V1 and 120 cells in V4) to train classifiers (see Methods).

In correct trials, both V1 and V4 populations decoded stimulus orientation significantly above chance (as determined by shuffling across stimulus conditions, with $P = 4 \times 10^{-5}$ for V1 and $P = 0.027$ for V4, Wilcoxon signed-rank test with FDR multiple comparison correction[28], using 200-ms sliding windows; Fig. 3a, left, and see the "Statistical analysis" section). However, in incorrect trials, only V1 neurons encoded stimuli significantly above chance ($P = 2.9 \times 10^{-4}$; Fig. 3a, right). In contrast, the V4 population was unable to distinguish between the stimuli in the task ($P = 0.58$). Decoder performance in V4 was not significantly different from that in V1 when tested on correct trials ($P = 0.3$), but was significantly different between the two areas when tested on incorrect trials ($P = 0.013$). That is, the stimulus-specific information required for a correct perceptual report was only present in V1, but not V4 (the results for each monkey are summarized in Supplementary Fig. 4a; $P < 0.01$ for monkey W and monkey C in correct trials in V1 and V4, and incorrect trials in V1; $P = 0.58$ for monkey W and $P = 0.88$ for

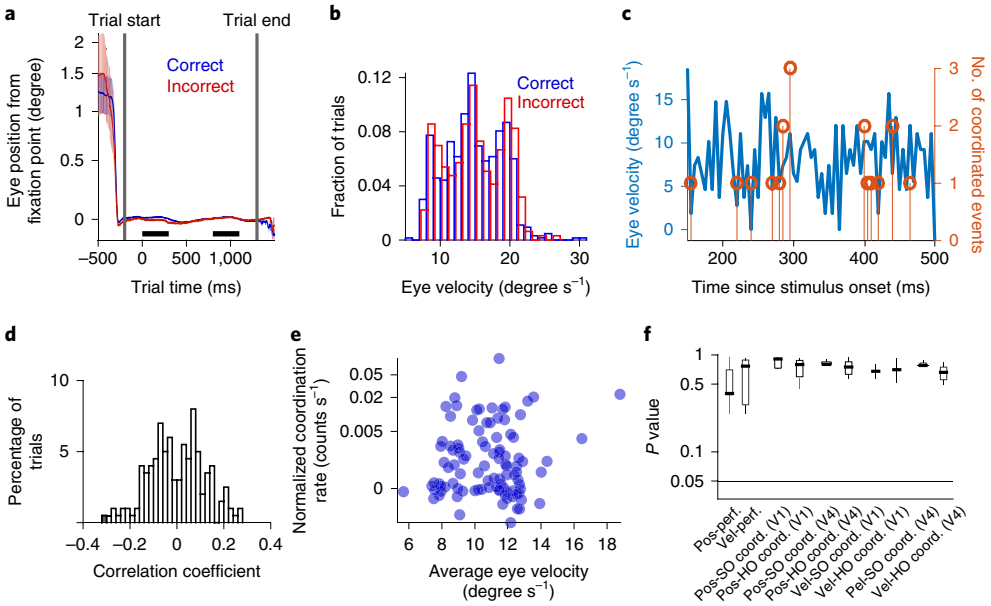

Fig. 6 | Coordination rates are unrelated to eye movements. a, Average traces of eye position relative to the fixation point, averaged across correct ($n=75$) and incorrect ($n=25$) trials in a sample session. The black bars represent the intervals when target and test stimuli are presented. **b**, Trial distributions of eye velocity for correct ($n=633$) and incorrect ($n=315$) trials are not significantly different ($P=0.54$, two-sided Wilcoxon rank-sum test). **c**, Single-trial trace of eye velocity (left *y* axis) and number of coordinated events (right *y* axis) for a sample trial as a function of time since test onset (the time bin is 5 ms). **d**, Distribution of Pearson's correlation coefficients of eye velocity and coordination rates, regardless of order, across trials ($n=948$) for all sessions ($P=0.3$, two-sided *t*-test). Only one trial in V1 and one trial in V4 showed significant ($P<0.05$) correlation coefficients. This analysis was performed by computing the CCG between the number of coordinated events and eye velocity (the two traces in **c**), averaged over trials across sessions (in V1 and V4). The CCGs were corrected for the slow co-fluctuations of the two variables by using a 50-ms smoothing kernel and subtracting the cross-correlation of smoothed traces from the original one. Each cross-correlation was *z*-scored before averaging. **e**, Trial-by-trial correlation of eye velocity and V1–V4 coordination, including second-order and higher-order events (calculated for the time lag of the peak V1–V4 coordination, as reported in the text). Trials were pooled from three representative sessions ($n=300$). Both eye velocity and coordination rates were *z*-scored before calculating the Pearson's correlation coefficient ($r=0.06$, $P=0.3$, two-sided *t*-test). **f**, Median *P* values for the eye position and eye movement control analyses and their correlation with coordination rates, averaged across sessions (V1: $n=22$, V4: $n=12$; results reported for the 300-ms test stimulus presentation). Pos-perf., difference between eye position in correct and incorrect trials (*P* value for two-sided Wilcoxon rank-sum test); Vel-perf., difference between eye velocity in correct and incorrect trials (*P* value for two-sided Wilcoxon rank-sum test); Pos-SO coord., Pearson's correlation between eye position and second-order (SO) coordination rates (separately for V1 and V4); Pos-HO coord., Pearson's correlation between eye position and higher-order (HO) coordination rates (separately for V1 and V4); Vel-SO coord., Pearson's correlation between eye velocity and SO coordination rates (separately for V1 and V4); Vel-HO coord., Pearson's correlation between eye velocity and HO coordination rates (separately for V1 and V4). For all Pearson correlations, the *P* value for the two-sided *t*-test was used. For each box plot, the middle bar represents the median, the box represents the 25th higher and lower percentiles, and the whiskers represent the range of the data points.

monkey C in incorrect trials in V4). It is noteworthy that this difference in decoding accuracy between V1 and V4 is not due to the different number of cells recorded in these areas. Although decoder performance typically increases with the number of cells[30,31], we recorded an approximately equal number of neurons in each area across sessions ($P=0.18$, Wilcoxon rank-sum test). Importantly, since firing rates in V1 and V4 were not significantly different between correct and incorrect trials (V1: $P=0.51$, V4: $P=0.79$; Fig. 3b; see also Supplementary Figs. 5, 6, and 7a), the lower decoder performance in area V4 in incorrect trials (compared to correct) cannot be due to differences in neuronal responses between these two conditions. Furthermore, to rule out fluctuations in attention as a confounding variable contributing to incorrect responses, we verified that in addition to firing rates, the Fano factor, noise correlations, and gamma power, which are typically correlated with attention[32,33], were not significantly different between correct and incorrect trials in V1 and V4 ($P>0.1$ for each comparison, Wilcoxon rank-sum test; Supplementary Fig. 7).

Coordinated spiking in V4 is correlated with perceptual accuracy. These results raise the possibility that in trials in which monkeys responded incorrectly, V4 neurons may not have encoded sensory information accurately due to impaired intracortical or cortico-cortical signaling (Fig. 3c). That is, incorrect trials may be associated with weaker temporal coordination between the spiking activity within V4, or between V1 and V4. To test this hypothesis, correct and incorrect trials in each session were separated to measure the correlation between coordinated spiking rates and the accuracy of perceptual reports (defined as percentage correct responses). The example session in Fig. 3d–f shows a subset of significantly occurring coordinated events in 9 V1 neurons and 12 V4 neurons for which coordination rates were significantly different between correct and incorrect trials ($P<0.01$, Wilcoxon rank-sum test). Surprisingly, whereas firing rates and pairwise coordination in V1 and V4 were unrelated to perceptual accuracy (Supplementary Fig. 1 describes additional cross-correlation analysis[34]), correct trials were associated with a clear increase in the frequency of occurrence of higher-order events in V4. In contrast, neuronal coordination in V1 did not appear to be related to behavioral decisions. Indeed, calculating the jitter-corrected coordination rates for correct and incorrect trials using a 300-ms sliding window with a 10-ms step (Fig. 3e–g; Supplementary Fig. 8) revealed that whereas the

temporal coordination between V1 neurons is unrelated to perceptual accuracy ($P=0.67$), high-order spiking coordination of V4 neurons carries information about perception during the presentation of the test stimulus ($P=0.002$, Wilcoxon rank-sum test). Indeed, in area V4, the mean number of significant high-order coordinated events is 11.32 for correct and 2.31 for incorrect trials (triplets: 3.7 for correct and 0.8 for incorrect; quartets: 5.6 for correct and 1.5 for incorrect; the rest of events have orders >4). In contrast, in area V1, correct trials were associated with a mean of 0.62 coordinated events (0.47 triplets and quartets, and 0.15 pairs), while incorrect trials were associated with 1.03 events (0.84 triplets and quartets, and 0.19 pairs).

The relationship between coordination rates in high-order ensembles and perceptual accuracy was a general phenomenon across sessions in both animals. We examined spiking coordination in V1 and V4 throughout the time course of a trial, and included only the significant events regardless of behavioral decision and ensemble size. This was done by calculating the mean difference in normalized coordination rates between correct and incorrect trials measured using a 300-ms window shifted in 10-ms increments, separately for pairwise and higher-order events (cumulating triplets and quartets), throughout the time course of a trial (statistical significance for the difference in coordination rates between correct and incorrect trials was assessed every 10 ms using the Wilcoxon signed-rank test). For pairs of neurons, coordination rates for correct and incorrect trials were highly variable but not significant for any time window (both in V1 and V4, $P=0.3$). In contrast, triplets and quartets in V4, but not V1, carried significant information about behavioral decisions following stimulus onset ($P<0.05$ throughout the 150–500-ms window relative to test onset; combining high-order coordinated events for each animal (monkey W: $P=0.001$, monkey C: $P=0.003$; Fig. 4a,b; Supplementary Fig. 4b shows the results per animal). Across sessions, we found a median high-order coordinated event count of 12.0 for correct and 8.03 for incorrect trials (coordination rates were highly variable across sessions and exponentially increasing with the number of neurons). Interestingly, the largest difference in coordination rates (correct versus incorrect) was observed for the window starting 150 ms after test onset (Fig. 4a), and not that covering the stimulus-onset transient. This goes against the idea that coordinated events are due to an increase in firing rate (fast modulation of firing rates is typically seen in the first 100 ms after stimulus onset). The difference in coordination rates (correct versus incorrect) between V1 and V4 was not significantly different for pairs of cells ($P=0.46$), but was significant for high-order events ($P=0.0032$).

The analysis of high-order coordination was restricted to neuronal ensembles up to size 4. Although we identified events of higher order than 4, they were seen in a limited number of sessions; hence, their frequency of occurrence was insufficient to assess statistical significance. However, it is probable that coordination rates may increase nonlinearly with the size of the neural population. Thus, the increase in spike timing coordination that we observed in small networks may be indicative of stronger, more pronounced neuronal coordination in larger networks. Importantly, analyzing the frequency of coordinated events during the target stimulus and delay period did not yield significantly different coordination rates in either V1 or V4 for any analysis window in either animal ($P>0.1$; Supplementary Figs. 4b and 9). Furthermore, shuffling spike trains within each trial abolished the difference in coordination rates between correct and incorrect trials (Supplementary Fig. 10).

We further performed an ideal observer analysis[35] to predict the perceptual accuracy of the animals on a trial-by-trial basis based on temporally coordinated events (Fig. 4c). For an example quartet in V4, the distributions of coordination rates for correct and incorrect trials were partially separated as the A_{ROC} was 0.66 (ref. [29]). In contrast, using the firing rates of the four example neurons and the coordination rates of the six possible pairs within the quartet revealed that the distributions of coordination rates for correct and incorrect trials largely overlapped (mean A_{ROC} for firing rates was 0.49, while for pairs it was 0.55; Fig. 4c). Across sessions, by calculating the A_{ROC} for the 150–500-ms time window after test onset, the difference in coordination rates was only significant for V4 triplets and quartets ($P=0.016$; Fig. 4d), but these effects were absent in V1 ($P=0.13$). In contrast, during the target stimulus or delay interval, coordination rates were unable to predict the accuracy of behavioral responses for any size of the neural ensemble ($P>0.1$).

Examining the temporal resolution of coordinated events may provide insight into underlying mechanisms. While converging inputs within 1 ms can effectively drive postsynaptic targets[3], coordination within the 10-ms range reflects multisynaptic communication between participating neurons[8]. Although our analysis focused on coordinated spiking within 5 ms, we varied the time bin of the analysis from 1 ms to 11 ms while holding the bin size at 5 ms and varying the jitter range from 3 ms to 13 ms. There were significant differences in coordination rates for time bins between 1 ms and 9 ms (Supplementary Fig. 11a) and jitter ranges >8 ms (Supplementary Fig. 11b), suggesting that coordinated events may reflect a combination of direct and multisynaptic interactions[8,26].

Spiking coordination between V1 and V4 neurons. Our results indicated that high-order coordinated events in V4, but not V1, are correlated with perceptual accuracy. However, areas V1 and V4 have both direct and indirect feedforward and feedback connections[36,37]. Since the absence of task-relevant stimulus information in V4 in incorrect trials (Fig. 3a) may be due to weak communication with V1, we further examined the functional significance of V1–V4 coordination. We focused on the test stimulus interval at which we had previously identified significant coordination in V4, and selected spike trains from simultaneously recorded V1 and V4 neurons with overlapping receptive fields ($n=8$ sessions). V4 spike trains were shifted relative to those in V1 by time τ (between −40 ms and 40 ms, using 5-ms increments). We examined spiking coordination between V1 and V4 populations by only including events for which the spikes of participating neurons originated from both areas. That is, at least one spike from each area should be generated for a coordinated event to be counted. By computing V1–V4 coordination rates as a function of τ (Fig. 5a), we identified the peak coordination rate (statistical significance determined by z-scoring coordination rates across τ values).

For 7 out of 8 sessions, we found a significant peak (z-score > 2) after stimulus onset for the difference between correct and incorrect coordination rates (Fig. 5b). This difference was most pronounced for higher-order, not pairwise, events and peaked when V4 lagged V1 by +25 ms (Fig. 5c). Surprisingly, while this is consistent with the delay of visual signals between V1 and V4 (ref. [38]), it indicates that information about perceptual accuracy is carried by feedforward, not feedback, pathways. Examining the peak frequency of feedforward (V1 to V4) coordination for pairwise and high-order events, we found that although pairwise spiking coordination was not different between correct and incorrect trials, high-order coordination (orders three and above) was correlated with behavioral outcome ($P<0.02$, Fig. 5d; pairwise coordination: $P=0.25$ in each animal; all high-order events combined: $P=0.0029$ for monkey W and 0.0004 for monkey C; see also Supplementary Fig. 4c for results in individual animals). Furthermore, we investigated whether high-order coordination events in V4 are triggered by high-order events in V1 or vice versa. Therefore, we computed the CCG between the times of occurrence of high-order events in V1 and V4. This analysis revealed a CCG peak at the +23 ms time lag to indicate that for correct trials, high-order coordination events in V4 occurred after V1 events (Fig. 5e). Incorrect trials were not associated with a significant CCG peak ($P=0.1$, t-test; for the difference between the

CCG peak in correct versus incorrect trials, $P=0.042$ for monkey W and $P=0.012$ for monkey C. Supplementary Fig. 12 shows the results of the pairwise CCG analysis).

Finally, we investigated whether high-order spiking coordination increases the firing rates of target neurons. Cross-correlation analysis was used to examine the relationship between high-order coordinated events in V1 and spiking activity in V4 and vice versa. We reasoned that if V1-coordinated events increase the firing rates in V4 via feedforward convergence of inputs, there should be a peak in the CCG corresponding to the conduction delay between V1 and V4 (approximately 30 ms). Furthermore, if V4-coordinated events increase the firing rates in V1 via feedback projections, there should be a corresponding peak in the CCG for negative time lags. However, we found no significant CCG peak for V1–V4 or V4–V1 convergence at any time lag, indicating that high-order spiking coordination does not increase firing rates in target neurons (Supplementary Fig. 13; Supplementary Fig. 14 shows CCGs corresponding to individual V4 neurons). These results are consistent with previous theoretical studies suggesting that spiking coordination increases local inhibition in the vicinity of target neurons to reduce the enhancing effect of the temporal summation of excitatory responses[18]. These results also confirm those from a cortico-cortical coordination study[3] in anesthetized monkeys showing that the effect of converging coordinated spikes on postsynaptic spike generation is only observed in monosynaptic communication across areas.

Coordinated events are unrelated to eye movements. Eye movements could potentially increase coordination rates. We addressed this issue by examining eye position traces, movements, and speed, and their relationship to behavioral performance and coordination rates. First, eye position was remarkably stable during fixation, and there was no difference between correct and incorrect trials. Across sessions, we did not observe slow drifting of eye position or differences associated with correct and incorrect trials ($P>0.1$, t-test, for all sessions in each animal; Fig. 6a). We also found that none of our sessions are characterized by a significant relationship between eye position and coordination rates ($P=0.13$ for all sessions, both for second order and higher-order events, in both V1 and V4). Second, the distributions of eye velocity were not significantly different between correct and incorrect trials ($P=0.5$, Wilcoxon rank-sum test, for all sessions; Fig. 6b). This indicates that monkeys do not employ different eye movement or position strategies when responding correctly or incorrectly. We further investigated the relationship between eye velocity and coordination rates by calculating velocity every 5 ms during the trial (Fig. 6c). Subsequently, we computed the correlation coefficient between the binned eye velocity and coordination rates. In area V4, correlation coefficients were not significant ($P>0.05$) for 99.5% of trials across sessions (Fig. 6d). These results held both for second order ($P=0.18$) and high-order coordination ($P=0.2$). Although coordinated events in V1 were unrelated to behavioral outcomes, we nonetheless examined the relationship between the number of events and eye velocity across trials, but found nonsignificant effects ($P>0.2$ for all sessions, both for second order and higher-order events). Third, we calculated the trial-by-trial correlation between V1–V4 coordinated events and eye velocity. Across sessions, there was a lack of significant correlation between these variables ($P>0.3$ across sessions, both for second order and higher-order events; Fig. 6e). Finally, we grouped together the median P values (across sessions) for the eye position and eye movement control analyses in relation to coordination rates (Fig. 6f). We conclude that oculomotor variables do not contribute to behavioral performance or spike timing coordination in V1 or V4.

Discussion

We discovered remarkably precise coordination of individual spike events in the visual cortex that are time locked to stimulus presentation. In contrast to previous studies in the retina[39], thalamus[40], infero-temporal cortex[41], and frontal cortex[42] revealing that spike timing carries stimulus-specific information, we found that high-order coordinated spiking events in the visual cortex influence perceptual accuracy in the absence of firing rate modulation, and without affecting stimulus coding. Furthermore, although high-order coordination was present in both the early and mid-level visual cortex, only V4 high-order coordination influenced perceptual accuracy. Surprisingly, despite the long-standing idea that cortico-cortical feedback projections carry information about behavior[8,43], we found that only feedforward spiking coordination is functionally relevant for perception. Thus, incorrect responses may be due to ineffective feedforward communication between sensory networks such that stimulus information may be lost along feedforward circuits[44].

Our results also indicate that incorrect behavioral reports can be due to poor stimulus decoding in area V4, but not V1. Although the firing rates of neurons were indistinguishable between correct and incorrect trials in these two areas, only V4 failed to encode task-relevant stimuli when trials were incorrect. This failure of sensory information to reach V4 could originate from weak intracortical and feedforward spiking coordination. Indeed, V1 signals must be accurately transmitted to V4 and other downstream areas to ensure accurate perception[45,46]. Consistent with previous theories that neuronal groups communicate via the precise temporal coordination of action potentials[47], we present empirical evidence that the accurate transmission of signals from V1 occurs via the precise temporal coordination between V1 and V4 and within V4 circuits. Furthermore, the increase in spiking coordination in V4 could contribute to effectively drive downstream networks to increase feedforward coordination to higher cortical areas to maintain accurate stimulus representations for visual perception.

One surprising finding is that feedforward, not feedback, cortico-cortical coordination is correlated with perceptual accuracy. Indeed, a commonly held idea is that extrastriate feedback to V1 carries top-down information about perceptual context[36]. Therefore, we expected that correct perceptual reports are associated with feedback, not feedforward, coordination. However, our results reveal that precise coordination in V4 occurs after coordinated spiking in V1, and that accurate perception is associated with elevated V1–V4 coordination. Neural mechanisms relying on feedforward spiking coordination are more efficient than feedback coordination, since the latter would cause a delay in transmitting sensory information to higher areas to influence behavior. This suggests that inter-areal spiking coordination might be optimized to facilitate efficient propagation of neural signals.

The absence of information regarding the identity of the neurons participating in coordinated spiking constitutes a limitation of our work. Indeed, to ensure reliable measurements, coordinated activity in each trial was calculated without defining ensemble 'words'; hence, exactly which spiking patterns among particular neuronal groups are most relevant for driving perception is unknown. However, complex network firing patterns may be accurately defined by the firing rates of neurons and the strength of population coupling[48], which is related to coordinated spiking. Additionally, computing word distributions from population recordings during wakefulness would be extremely difficult given our finite time trial structure and session length.

Our results indicate that coordinated events in V4 are probably due to V1 coordination propagated along feedforward pathways. Alternatively, V1–V4 coordination could reflect a common drive from an external source enhancing coordination in each area separately. However, this is unlikely to be the case. Indeed, our cross-correlation analysis of coordinated events revealed a peak at the expected temporal delay between V1 and V4 signals[36]. Although area V2 is a major recipient of inputs from V1, and is likely to

mediate or contribute to V4 coordination[46], it is unlikely to mediate coordinated spiking in V1. That is, if V2 neurons were the common source of coordination in V1 and V4, we would have observed that coordinated spiking in V1 and V4 occurs almost simultaneously, which is contrary to our observations.

One possible concern in our study is cortical state. Indeed, during wakefulness, the visual cortex randomly fluctuates between different states of synchrony[30], and the state of local V4 populations affects behavioral performance. However, while cortical state could alter the strength of coordination, it would probably increase coordination at long timescales rather than the near-coincident coordinated spiking (within 5 ms) reported here. Nonetheless, this is not a serious concern in our study, since the long timescale coordination was in fact removed as part of our controls when the jittered coordination rate was subtracted from the raw coordination rate (see Methods). Furthermore, we have previously reported[30] that an increase in low-frequency synchrony in local populations decreases perceptual accuracy, whereas spiking coordination, our measure of fast timescale synchrony, increases it. Cortical state could also fluctuate during slow changes in behavioral performance during the session. However, when examining the relationship between coordination rates and history of perceptual performance (percentage of correct reports in past trials), we failed to observe significant correlations ($P > 0.1$; Supplementary Fig 15).

Our results suggest that the brain may employ different strategies to encode sensory stimuli and to preserve perceptual accuracy during a behavioral task. While the presence of incoming stimuli increases both firing rates and spiking coordination in the visual cortex, only rate modulation is related to sensory coding. In contrast, perceptual accuracy is correlated with precise spiking coordination regardless of firing rate modulation. This argues for complementary functions served by the precise coordination of spike events and discharge rates in the visual cortex. A relatively similar mechanism has been previously proposed in the primary motor cortex[49], whereby spike synchronization and rate modulation were found to be differentially involved in motor processing. Furthermore, given the similarities of the microcircuitry underlying different sensory modalities[50], spiking coordination could constitute a ubiquitous mechanism of information coding extending beyond vision and influencing a wide range of cognitive functions.

Online content

Any methods, additional references, Nature Research reporting summaries, source data, statements of code and data availability and associated accession codes are available at https://doi.org/10.1038/s41593-019-0406-3.

Received: 3 January 2018; Accepted: 10 April 2019;
Published online: 20 May 2019

References

1. Averbeck, B. B., Latham, P. E. & Pouget, A. Neural correlations, population coding and computation. *Nat. Rev. Neurosci.* **7**, 358–366 (2006).
2. Shadlen, M. N. & Newsome, W. T. The variable discharge of cortical neurons: implications for connectivity, computation, and information coding. *J. Neurosci.* **18**, 3870–3896 (1998).
3. Zandvakili, A. & Kohn, A. Coordinated neuronal activity enhances corticocortical communication. *Neuron* **87**, 827–839 (2015).
4. Heinzle, J., König, P. & Salazar, R. F. Modulation of synchrony without changes in firing rates. *Cogn. Neurodyn.* **1**, 225–235 (2007).
5. Trousdale, J., Hu, Y., Shea-Brown, E. & Josić, K. A generative spike train model with time-structured higher order correlations. *Front. Comput. Neurosci.* **7**, 84 (2013).
6. Abeles, M. *Corticonics: Neural Circuits of the Cerebral Cortex*. (Cambridge Univ. Press, 1991).
7. Dan, Y., Alonso, J. M., Usrey, W. M. & Reid, R. C. Coding of visual information by precisely correlated spikes in the lateral geniculate nucleus. *Nat. Neurosci.* **1**, 501–507 (1998).
8. Takeuchi, D., Hirabayashi, T., Tamura, K. & Miyashita, Y. Reversal of interlaminar signal between sensory and memory processing in monkey temporal cortex. *Science* **331**, 1443–1447 (2011).
9. Uhlhaas, P. et al. Neural synchrony in cortical networks: history, concept and current status. *Front. Integr. Neurosci.* **3**, 17 (2009).
10. Singer, W. & Gray, C. M. Visual feature integration and the temporal correlation hypothesis. *Annu. Rev. Neurosci.* **18**, 555–586 (1995).
11. Histed, M. H. & Maunsell, J. H. R. Cortical neural populations can guide behavior by integrating inputs linearly, independent of synchrony. *Proc. Natl Acad. Sci. USA* **111**, E178–E187 (2013).
12. Alonso, J. M., Usrey, W. M. & Reid, R. C. Precisely correlated firing in cells of the lateral geniculate nucleus. *Nature* **383**, 815–819 (1996).
13. Bruno, R. M. & Sakmann, B. Cortex is driven by weak but synchronously active thalamocortical synapses. *Science* **312**, 1622–1627 (2006).
14. Salinas, E. & Sejnowski, T. J. Impact of correlated synaptic input on output firing rate and variability in simple neuronal models. *J. Neurosci.* **20**, 6193–6209 (2000).
15. Renart, A. et al. The asynchronous state in cortical circuits. *Science* **327**, 587–590 (2010).
16. Wehr, M. & Zador, A. M. Balanced inhibition underlies tuning and sharpens spike timing in auditory cortex. *Nature* **426**, 442–446 (2003).
17. Gabernet, L., Jadhav, S. P., Feldman, D. E., Carandini, M. & Scanziani, M. Somatosensory integration controlled by dynamic thalamocortical feed-forward inhibition. *Neuron* **48**, 315–327 (2005).
18. Fries, P. Neuronal gamma-band synchronization as a fundamental process in cortical computation. *Annu. Rev. Neurosci.* **32**, 209–224 (2009).
19. Ecker, A. S. et al. State dependence of noise correlations in macaque primary visual cortex. *Neuron* **82**, 235–248 (2014).
20. Salazar, R. F., Dotson, N. M., Bressler, S. L. & Gray, C. M. Content-specific fronto-parietal synchronization during visual working memory. *Science* **338**, 1097–1101 (2012).
21. Bosman, C. A. et al. Attentional stimulus selection through selective synchronization between monkey visual areas. *Neuron* **75**, 875–888 (2012).
22. van Kerkoerle, T. et al. Alpha and gamma oscillations characterize feedback and feedforward processing in monkey visual cortex. *Proc. Natl Acad. Sci. USA* **111**, 14332–14341 (2014).
23. Jia, X., Smith, M. A. & Kohn, A. Stimulus selectivity and spatial coherence of gamma components of the local field potential. *J. Neurosci.* **31**, 9390–9403 (2011).
24. Schroeder, C. E., Mehta, A. D. & Givre, S. J. A spatiotemporal profile of visual system activation revealed by current source density analysis in the awake macaque. *Cereb. Cortex* **8**, 575–592 (1998).
25. Hansen, B. J., Chelaru, M. I. & Dragoi, V. Correlated variability in laminar cortical circuits. *Neuron* **76**, 590–602 (2012).
26. Pipa, G., Wheeler, D. W., Singer, W. & Nikolić, D. NeuroXidence: reliable and efficient analysis of an excess or deficiency of joint-spike events. *J. Comput. Neurosci.* **25**, 64–88 (2008).
27. Schneidman, E., Berry, M. J., Segev, R. & Bialek, W. Weak pairwise correlations imply strongly correlated network states in a neural population. *Nature* **440**, 1007–1012 (2006).
28. Benjamini, Y. & Hochberg, Y. Controlling the false discovery rate: a practical and powerful approach to multiple testing. *J. R. Stat. Soc. Ser. B* **57**, 289–300 (1995).
29. Britten, K. H., Newsome, W. T., Shadlen, M. N., Celebrini, S. & Movshon, J. A. A relationship between behavioral choice and the visual responses of neurons in macaque MT. *Vis. Neurosci.* **13**, 87 (2009).
30. Beaman, C. B., Eagleman, S. L. & Dragoi, V. Sensory coding accuracy and perceptual performance are improved during the desynchronized cortical state. *Nat. Commun.* **8**, 1–14 (2017).
31. Gutnisky, D. A., Beaman, C., Lew, S. E. & Dragoi, V. Cortical response states for enhanced sensory discrimination. *eLife* **6**, e29226 (2017).
32. Cohen, M. R. & Maunsell, J. H. R. Attention improves performance primarily by reducing interneuronal correlations. *Nat. Neurosci.* **12**, 1594–1601 (2009).
33. McAdams, C. J. & Maunsell, J. H. R. Effects of attention on the reliability of individual neurons in monkey visual cortex. *Neuron* **23**, 765–773 (1999).
34. Bair, W., Zohary, E. & Newsome, W. T. Correlated firing in macaque visual area MT: time scales and relationship to behavior. *J. Neurosci.* **21**, 1676–1697 (2001).
35. Emmerich, D. S. *Signal Detection Theory and Psychophysics* by David M. Green, John A. Swets. *Q. Rev. Biol.* **42**, 578 (1967).
36. Ungerleider, L. G., Galkin, T. W., Desimone, R. & Gattass, R. Cortical connections of area V4 in the macaque. *Cereb. Cortex* **18**, 477–499 (2008).
37. Markov, N. T. et al. Anatomy of hierarchy: feedforward and feedback pathways in macaque visual cortex. *J. Comp. Neurol.* **522**, 225–259 (2014).
38. Lee, J., Williford, T. & Maunsell, J. H. Spatial attention and the latency of neuronal responses in macaque area V4. *J. Neurosci.* **27**, 9632–9637 (2007).
39. Gollisch, T. & Meister, M. Rapid neural coding in the retina with relative spike latencies. *Science* **319**, 1108–1111 (2008).

40. Dan, Y., Atick, J. J. & Reid, R. C. Efficient coding of natural scenes in the lateral geniculate nucleus: experimental test of a computational theory. *J. Neurosci.* **16**, 3351–3362 (1996).
41. Hirabayashi, T. & Miyashita, Y. Dynamically modulated spike correlation in monkey inferior temporal cortex depending on the feature configuration within a whole object. *J. Neurosci.* **25**, 10299–10307 (2005).
42. Vaadia, E. et al. Dynamics of neuronal interactions in monkey cortex in relation to behavioural events. *Nature* **373**, 515–518 (1995).
43. Gilbert, C. D. & Li, W. Top-down influences on visual processing. *Nat. Rev. Neurosci.* **14**, 350–363 (2013).
44. Smolyanskaya, A., Haefner, R. M., Lomber, S. G. & Born, R. T. A modality-specific feedforward component of choice-related activity in MT. *Neuron* **87**, 208–219 (2015).
45. Crick, F. & Koch, C. Constraints on cortical and thalamic projections: the no-strong-loops hypothesis. *Nature* **391**, 245–250 (1998).
46. Felleman, D. J. & Van Essen, D. C. Distributed hierarchical processing in the primate cerebral cortex. *Cereb. Cortex.* **1**, 1–47 (1991).
47. Fries, P. A mechanism for cognitive dynamics: neuronal communication through neuronal coherence. *Trends Cogn. Sci.* **9**, 474–480 (2005).
48. Okun, M. et al. Population rate dynamics and multineuron firing patterns in sensory cortex. *J. Neurosci.* **32**, 17108–17119 (2012).
49. Riehle, A. Spike synchronization and rate modulation differentially involved in motor cortical function. *Science* **278**, 1950–1953 (1997).
50. Yang, Y. & Zador, A. M. Differences in sensitivity to neural timing among cortical areas. *J. Neurosci.* **32**, 15142–15147 (2012).

Acknowledgements

The authors thank X. Pitkow, H. Shouval, and J. Magnotti for discussions and comments. This work was supported by NIH EUREKA and NEI grants to V.D.

Author contributions

A.R.A., M.H., and V.D. designed the experiments. A.R.A. and M.H. performed the experiments. N.S. analyzed the data with guidance from V.D. N.S. and V.D. wrote the manuscript.

Competing interests

The authors declare no competing interests.

Additional information

Supplementary information is available for this paper at https://doi.org/10.1038/s41593-019-0406-3.

Reprints and permissions information is available at www.nature.com/reprints.

Correspondence and requests for materials should be addressed to V.D.

Publisher's note: Springer Nature remains neutral with regard to jurisdictional claims in published maps and institutional affiliations.

Methods

All experiments were performed under protocols approved by The University of Texas at Houston Animal Care and Use Committee. Two adult male rhesus monkeys (*Macaca mulatta*; monkey C: 15 kg, 12 years old; monkey W: 13 kg, 15 years old) were used in the experiments. A titanium head post was implanted in the medial frontal region with the help of multiple anchor screws. Following a recovery period of about 10 days, the monkeys were trained for 3–4 months on visual fixation and discrimination tasks. After the monkeys learned the tasks, two 19-mm inner diameter recording chambers (Crist Instruments) were implanted in areas V1 and V4 of each monkey (according to a MRI map). A few stainless-steel screws were inserted into the skull around the recording chamber, and a thin stainless steel wire was wrapped around the screws for additional support. General information about the methodology used in this study is provided in the Nature Research Reporting Summary. More detailed information is provided below.

Behavioral task. The two monkeys were required to hold fixation within a window of 1° in diameter throughout stimulus presentation. Eye movements were monitored throughout the recording session using an infrared eye tracking system (EyeLink II, SR Research) at a 1-kHz sampling rate. The eye position was calibrated at the beginning of each experiment using a five-point calibration procedure. The eye-tracker gains were adjusted so that they were linear for horizontal and vertical eye deflections. The fixation pattern was carefully analyzed offline. Microsaccades were analyzed every 10 ms by using a vector velocity threshold of $10°\,s^{-1}$ (this corresponds to a 0.1° eye movement between consecutive 10-ms intervals). If a detected microsaccade exceeded 0.25° (fixation instability), the trial was automatically aborted. Once the animal achieved stable fixation for 200 ms, a 300-ms target stimulus was flashed, and then after a 500–1,200-ms delay consisting of a blank screen, a test stimulus was flashed for 300 ms (fixation was required for an extra 200 ms after the offset of the test stimulus for the trial to be considered valid). In approximately half of the trials, the test stimulus had the same orientation as that of the target (match condition). In the other half of the trials, the test orientation was rotated from the target by 3° for monkey C and 5° for monkey W (non-match condition; the test orientation was chosen to be close to the image discrimination threshold for each monkey, as determined at the beginning of each experiment). The animals were trained to release a bar on match trials and to hold the bar on non-match trials to receive a juice reward. Match and non-match trials were randomly interleaved (we collected at least 400 trials in each session). The inter-trial interval was 10 s. All stimuli were presented at parafoveal locations (4–6° eccentricity and away from the vertical and horizontal meridians) and consisted of circular monochromic natural scenes with a diameter of 8–10°. Only one image was presented in each session. The image varied between experimental sessions but was kept unchanged during each recording session. The stimulus location and size were optimized in each session to ensure that the largest number of simultaneously recorded cells was stimulated in both areas. Stimulus presentation was recorded and synchronized with the neural data using an Experiment Control Module programmable device (FHC Inc.). The correct response was to release the bar for match trials and keep holding it for 1 s or longer for non-match trials. The response was detected using an impedance detector (Crist Instrument response box). If the monkey responded correctly, he was rewarded with five drops of diluted apple juice (Crist Inc.).

Electrophysiological recordings. We performed electrical recordings in areas V1 and V4 using linear arrays (16 channels, Plexon U-probes) with contacts spacing at 100 µm advanced using a NAN drive system (NAN Instruments) attached to the recording chamber. In each session, we advanced a maximum of two linear arrays into each cortical area (we performed 26 recording sessions, and recorded up to 14 units per area simultaneously in each session). The average number of cells per session was as follows: V1: 8 ± 3; V4: 10 ± 4. The distributions of the number of cells per session in V1 and V4 were not significantly different ($P = 0.18$, Wilcoxon rank-sum test). Both the target and test stimuli fully covered the receptive field of cells. Cells unresponsive to the visual stimuli ($P > 0.05$) were excluded from the analysis. Real-time neuronal signals were processed using a Multichannel Acquisition Processor system (Plexon Inc.) at a sampling rate of 40 kHz. The signals were first filtered by a preamplifier box into spike channels (150 Hz to 8 kHz, 1 pole low-cut, 3 pole high-cut, with programmable referencing, ×50 gain) and field potential channels (0.07, 0.7, 3–170, 300, 500 Hz user-selectable, 1 pole low-cut, 1 pole high-cut, ×50 gain). Single-unit signals were further amplified, filtered, and viewed on an oscilloscope, and heard through a speaker. The spike waveforms that were above the threshold were saved and fine sorted after data acquisition was terminated using Plexon's offline sorter program. After a unit was isolated, its receptive field was mapped with dynamic gratings or using reverse correlation while the animal maintained fixation. Waveforms that crossed a predefined threshold (~4 standard deviations above the amplitude of the noise signal) were stored for offline analyses. Spike waveforms were manually processed using Plexon's offline sorter program and waveform clustering parameters, such as principle component analysis, along with spike amplitude, timing, width, valley, and peak. Single units were subsequently analyzed using custom scripts in MATLAB. After performing spike sorting, we found a total of six electrode contacts with more than one identified cell (in six of the sessions). Eliminating the 'extra' cell for one electrode contact yielded results that differed in magnitude by <0.91% from those originally reported in the manuscript (in Figs. 1h, 2e,f, 3a, 4b, and 5c–e). Sorted spikes were further analyzed for firing rates for the time course of the trial for which fixation was stable (200 ms before the target stimulus and 200 ms after the test stimulus). The peri-stimulus spike time histograms (PSTHs) of spikes were generated by averaging the spike trains binned at 1 ms for the time course of the trial. Stimulus presentation was controlled with custom scripts using PsychoToolBox. Synchronization between multiple devices (eye tracker, juicer, and graphic card) was controlled by the Experimental Control Module (FHC Inc.) to ensure the best timing accuracy.

Coordination rates. The frequency of occurrence of coordinated events (coordination rate) was calculated using the tool NeuroXidence[26]. The core of the method is the identification of coordinated patterns consisting of synchronized spikes from specific neurons. For example, pattern $p = x1xx1xxxx1$ indicates the occurrence of spikes emitted by the second, fifth, and tenth neuron from a set of ten cells; the other neurons may or may not fire spikes (x indicates 0 or 1). The size of the time bin in which spiking patterns are identified determines the temporal accuracy of coordinated spiking. For the analysis in the manuscript, we chose a time bin of 5 ms; that is, the relative timing between all the spikes in a bin was <5 ms. However, it is possible that certain spikes with a relative timing less than the bin width could occur in adjacent bins, which means that their coordinated pattern cannot be detected. To correct for this issue[26], each spike was replicated into the adjacent time bin before identifying specific spiking patterns. After identifying patterns using replicated spikes, if a spiking pattern is repeated in an adjacent time bin, the repeated copy is removed[26]. After identifying all patterns p, the coordination rate in trial j is calculated as $F_j^p = \frac{\text{No. of occurrences of pattern } p}{t}$, where t is the length of the time window in which patterns were detected (for instance the length of the trial).

To determine whether pattern p occurs significantly more often than chance level (or more frequently than expected by fast fluctuations in the firing rates of neurons or co-fluctuations of firing rates of multiple neurons), the distribution of F_j^p across trials was tested against the null hypothesis[26]. The null hypothesis was generated by shifting each spike train by a random time, which is the jittering range. The jittering range is shorter than the time scale of possible co-fluctuations of firing rates, but longer than a single time bin. In our analysis, the mean value of the jittering range was 10 ms. The jitter-corrected coordination rates were calculated[26] as $\Delta F_j^p = F_j^p(\text{original}) - F_j^p(\text{null})$, which was tested to be significantly >0 (with $P < 0.01$, Wilcoxon signed-rank test, by comparing the original and jittered coordination rates, using the FDR multiple comparison correction; we used 20 jitters and averaged the coordination rates across all the jitters). The comparison between the original and jittered coordination rates was tested across trials for each neuronal combination (we used the same methodology as in a previous study[26]). Throughout the manuscript, we report the jitter-corrected coordination rate as the coordination rate. When comparing between two conditions (for example, stim1 versus stim2, as in Fig. 1h), the significance of the coordination rate for each pattern was determined separately for each condition. To avoid the effect of unbalanced sets of trials on the power of statistical tests, bootstrapped distributions were generated as follows: trial sets in each condition were resampled with replacement (the sample size was 100), then the P value of the Wilcoxon signed-rank test was calculated for each sample set. This procedure was repeated to obtain a distribution of P values from which the mean P value was compared with the threshold level ($\alpha = 0.01$). The FDR-corrected α threshold varied between 0.016 and 0.039 across sessions. However, we conservatively and uniformly applied the FDR correction and used an even lower threshold, $\alpha = 0.01$, for the entire dataset when assessing the statistical significance.

Finally, the coordination rate combined across patterns of size c in trial j (c is the number of spikes within the pattern; for example, for coordinated pairs $c = 2$, for triplets $c = 3$, and so on) was calculated as $F_j(c) = \frac{\sum_p \Delta F_j^p}{N_c}$, where the numerator represents the sum of statistically significant coordination rates for all patterns of size c, and the denominator, N_c, is the total number of possible patterns of size c (regardless of significance). For example, if ten neurons were recorded, the sum of coordination rates for pairs was divided by $N_2 = 45$ (which is equal to $C_{10}{}^2$), for triplets by $N_3 = 120$ ($C_{10}{}^3$), and for quartets by $N_4 = 210$ ($C_{10}{}^4$). The reason for reporting normalized values instead of actual rates (for example, Fig. 4) was to be able to compare coordination rates across assembly sizes (pairs versus triplets versus quartets, and so on) and across sessions with varying numbers of recorded neurons. At the end, the coordination rates of size c were averaged across trials for each condition.

To compare coordination rates across two conditions (as in Fig. 1h or Fig. 4a,b), we first calculated $F_j(c)$ using all the patterns of size c that were significantly occurring in at least one of the two conditions, then compared the distribution of $F_j(c)$ across trials in condition 1 with the distribution of $F_j(c)$ across trials in condition 2 using the Wilcoxon rank-sum test (the multiple-comparison correction of the P values is described in the 'Statistical analysis' section below). For the sliding window analysis shown in Fig. 4a, this procedure was repeated for each analysis window, and then each P value of the rank-sum test was plotted.

Spike train simulation. We generated spike trains that mimicked the firing rates of the experimental neurons but lacked coordinated spiking. This was done by generating independent spike trains with the same statistics as real neurons using a Poisson process for which the rate of events in any 1-ms time bin was the trial-averaged firing rate of the experimental neuron. Using this procedure, we generated the exact same number of trials and neurons as in the experimental data such that the PSTH of each simulated neuron matched the PSTH of the corresponding experimental neuron. To generate spike trains with, for example, 20% shared spikes among neurons, we generated independent spike trains so that the firing rates were 20% lower than the experimentally measured firing rates. We subsequently added the shared spikes across the entire population to provide a match for the spike rates of the actual neurons (but with random spike timing within a ±25 ms window; Fig. 2a). As a result, the trial-averaged firing rates of the simulated neurons matched their corresponding real neurons (Fig. 2b) while the spike count correlation increases monotonically with the percentage of shared spikes (Fig. 2c).

Support vector machine decoder. We used a linear support vector machine decoder[51] to determine whether the population firing rates in V1 or V4 carry information about visual stimuli and/or perceptual accuracy (using quadratic and radial basis function kernel functions yields similar results). Specifically, we computed the mean firing rates of each neuron in the population for the specified time window in each trial, and then classified the population response using binary labels specifying the condition of the trial (for example, stim1 versus stim2). To train the decoder (that is, to tune the parameters of the kernel function of the decoder), we used 80% of the correct trials in a given session. To test the decoder, we used the rest of the 20% of trials from each corresponding condition (correct or incorrect), and cross-validation was done by testing sets of trials different from those used during training (separately for the correct and incorrect conditions)[25,30,31]. Decoder performance was calculated as the percentage of correctly classified test trials. This procedure (decoder training and testing) was repeated 1,000 times, each time using a random subset of the corresponding trials for training and the rest of them for testing (separately for each condition). As a control, we trained decoders with randomly shuffled class labels (1,000 random shuffles). The performance of the shuffled decoder was used as a null hypothesis for the statistical test of decoder performance. To test the robustness of our decoding analysis, we additionally used a decoder for which both correct and incorrect trials were used for training (same number of correct and incorrect trials), and then decoding performance was tested by using either the rest of the 20% correct or incorrect trials. The test trials were different from the set of training trials, and we repeated the decoder analysis 1,000 times and generated randomly shuffled labels as described above. However, this decoder yielded results that were similar to those for which only the correct trials were used during training despite the fact that the mean decoder performance was about 2% lower compared with original decoding performance, when training was performed using correct trials only (that is, 53% versus 55% in V1, and 55% versus 58% in V4, for the time window that maximizes decoder performance). That is, decoding performance in V1 was significantly higher than chance for both correct and incorrect trials ($P=4\times10^{-5}$ for correct and $P=2.9\times10^{-5}$ for incorrect). Decoding performance in V4 was significantly higher than chance for correct trials ($P=0.027$), but indistinguishable from chance for incorrect trials ($P=0.58$).

Statistical analysis. To determine the statistical significance of our results, we used the two-sided Wilcoxon signed-rank test, unless the name of the test is indicated next to the *P* value. We chose this test rather than parametric tests, such as the *t*-test, for its greater statistical power (lower type I and type II errors) when data are not normally distributed[52,53]. The normality of the data distribution was not formally tested. To minimize type I and type II errors, when multiple groups of data were tested, we used the FDR multiple comparison correction[28]. Compared to Bonferroni, which is the most conservative multiple comparison correction, FDR has greater statistical power. Technically, FDR controls the probability that a rejected statistical test is, in fact, falsely rejected. In practice, to apply FDR to multiple *P* values, we used an implementation of the Benjamini–Hochberg procedure to determine a new threshold for the *P* value. The statistical significance was then determined by comparing each *P* value to the new threshold instead of the original threshold (usually set to 0.05). The FDR multiple comparison correction was applied for the entire dataset whenever multiple groups of data were tested, including the statistical significance assessment of coordination rates for each neuronal combination in each cortical area. No statistical methods were used to predetermine sample sizes, but our sample sizes were similar to those reported in previous publications[19,30–33,49]. Data collection and analyses were not performed blind to the conditions of the experiments.

Reporting Summary. Further information on research design is available in the Nature Research Reporting Summary linked to this article.

Data availability

The data that support the findings of this study are available from the corresponding author upon reasonable request.

Code availability

The custom-written software supporting the findings of this study is available from the corresponding author upon reasonable request.

References

51. Bishop C. M. *Pattern Recognition and Machine Learning* (Springer, 2006).
52. N. Haidous, N. & S. Sawilowsky, S. Robustness and power of the Kornbrot rank difference, signed ranks, and dependent samples *T*-test. *Am. J. Appl. Math. Stat.* **1**, 99–102 (2013).
53. Sawilowsky, S. S. & Blair, R. C. A more realistic look at the robustness and Type II error properties of the *t* test to departures from population normality. *Psychol. Bull.* **111**, 352–360 (1992).

nature research

Corresponding author(s): Valentin Dragoi

Last updated by author(s): Mar 29, 2019

Reporting Summary

Nature Research wishes to improve the reproducibility of the work that we publish. This form provides structure for consistency and transparency in reporting. For further information on Nature Research policies, see Authors & Referees and the Editorial Policy Checklist.

Statistics

For all statistical analyses, confirm that the following items are present in the figure legend, table legend, main text, or Methods section.

n/a	Confirmed	
☐	☒	The exact sample size (*n*) for each experimental group/condition, given as a discrete number and unit of measurement
☐	☒	A statement on whether measurements were taken from distinct samples or whether the same sample was measured repeatedly
☐	☒	The statistical test(s) used AND whether they are one- or two-sided *Only common tests should be described solely by name; describe more complex techniques in the Methods section.*
☐	☒	A description of all covariates tested
☐	☒	A description of any assumptions or corrections, such as tests of normality and adjustment for multiple comparisons
☐	☒	A full description of the statistical parameters including central tendency (e.g. means) or other basic estimates (e.g. regression coefficient) AND variation (e.g. standard deviation) or associated estimates of uncertainty (e.g. confidence intervals)
☐	☒	For null hypothesis testing, the test statistic (e.g. *F*, *t*, *r*) with confidence intervals, effect sizes, degrees of freedom and *P* value noted *Give P values as exact values whenever suitable.*
☒	☐	For Bayesian analysis, information on the choice of priors and Markov chain Monte Carlo settings
☒	☐	For hierarchical and complex designs, identification of the appropriate level for tests and full reporting of outcomes
☐	☒	Estimates of effect sizes (e.g. Cohen's *d*, Pearson's *r*), indicating how they were calculated

Our web collection on statistics for biologists contains articles on many of the points above.

Software and code

Policy information about availability of computer code

Data collection	Plexon MAP server, Eyelink II controller, FHC experimental control module, custom-written PsychToolbox script as well as custom made Matlab 2008 programs were used.
Data analysis	Plexon offline sorter v3 and Matlab 2011a-2016b were used.

For manuscripts utilizing custom algorithms or software that are central to the research but not yet described in published literature, software must be made available to editors/reviewers. We strongly encourage code deposition in a community repository (e.g. GitHub). See the Nature Research guidelines for submitting code & software for further information.

Data

Policy information about availability of data

All manuscripts must include a data availability statement. This statement should provide the following information, where applicable:

- Accession codes, unique identifiers, or web links for publicly available datasets
- A list of figures that have associated raw data
- A description of any restrictions on data availability

The data that support the findings of this study are available from the corresponding author on reasonable request (V.D.).

Field-specific reporting

Please select the one below that is the best fit for your research. If you are not sure, read the appropriate sections before making your selection.

☒ Life sciences ☐ Behavioural & social sciences ☐ Ecological, evolutionary & environmental sciences

Life sciences study design

All studies must disclose on these points even when the disclosure is negative.

Sample size	We conducted this study with two monkeys in order to achieve robustness for the behavioral and electrophysiological results despite possible differences in the behavioral strategies between monkeys (all results were consistent across animals). We limited the number of monkeys to two to meet the requirements of lab animal use regulations that requires minimizing the number of animals in each study. Choosing the sample size of two is typical in electrophisiological studies in monkeys.
Data exclusions	No exclusion in the choice of data were made. If data points were excluded further in the analysis, we carefully explain the criteria in the manuscript.
Replication	The experiments were repeated up to 30 times in each animal. All of the finding are reproducible. The experimental equipment is commercially available and the custom made software and codes for reproduction of the analyses are available upon request.
Randomization	Not applicable to this study. Two subjects were not categorized or randomly assigned. The same experiments were repeated in both animals.
Blinding	Since no group allocation was done in this study, blinding was not required.

Reporting for specific materials, systems and methods

We require information from authors about some types of materials, experimental systems and methods used in many studies. Here, indicate whether each material, system or method listed is relevant to your study. If you are not sure if a list item applies to your research, read the appropriate section before selecting a response.

Materials & experimental systems

n/a	Involved in the study
☒	☐ Antibodies
☒	☐ Eukaryotic cell lines
☐	☒ Palaeontology
☐	☒ Animals and other organisms
☒	☐ Human research participants
☒	☐ Clinical data

Methods

n/a	Involved in the study
☒	☐ ChIP-seq
☒	☐ Flow cytometry
☒	☐ MRI-based neuroimaging

Palaeontology

Specimen provenance	We did not used any specimen
Specimen deposition	We did not used any specimen
Dating methods	We did not used any dating method

☐ Tick this box to confirm that the raw and calibrated dates are available in the paper or in Supplementary Information.

Animals and other organisms

Policy information about studies involving animals; ARRIVE guidelines recommended for reporting animal research

Laboratory animals	Two adult male rhesus monkeys (Macaca mulatta) were used. Monkey C (age 12) had 15 kg, and monkey W (age 15) had 13 kg.
Wild animals	We did not include wild animals.
Field-collected samples	We did not include field collected samples.
Ethics oversight	The animal experimentation was done under supervision of the Center for the Lab Animal Medicine and Care, at the University of Texas Health Science Center at Houston and the protocols were reviewed by the Animal Welfare Committee at the same institution.

Note that full information on the approval of the study protocol must also be provided in the manuscript.